4-17-2014

Investigation of Hidden Periodic Structures on SEM Images of Opal-like Materials Using FFT and IFFT

Nicolas Stephant
University of Nantes

Benjamin Rondeau
University of Nantes

Jean-Pierre Gauthier
Centre de Recherches Gemmologiques, Nantes

Jason A. Cody
Lake Forest College, cody@lakeforest.edu

Citation

N. Stephant, B. Rondeau, J. P. Gauthier, J. A. Cody, E. Fritsch, "Investigation of hidden periodic structures on SEM images of opal-like materials using FFT and IFFT," Scanning, 2014, 36, 487-499.

SCANNING VOL. 36, 487–499 (2014)

Investigation of Hidden Periodic Structures on SEM Images of Opal-Like Materials Using FFT and IFFT

Nicolas Stephant,[1] Benjamin Rondeau,[2] Jean-Pierre Gauthier,[3] Jason A. Cody,[4] and Emmanuel Fritsch[1]

[1]Institut des Matériaux Jean Rouxel, University of Nantes, Nantes, France
[2]Laboratoire de Planétologie et Géodynamique, University of Nantes, Nantes, France
[3]Centre de Recherches Gemmologiques, Nantes, France
[4]Department of Chemistry, Lake Forest College, Lake Forest, Illinois

Summary: We have developed a method to use fast Fourier transformation (FFT) and inverse fast Fourier transformation (IFFT) to investigate hidden periodic structures on SEM images. We focused on samples of natural, play-of-color opals that diffract visible light and hence are periodically structured. Conventional sample preparation by hydrofluoric acid etch was not used; untreated, freshly broken surfaces were examined at low magnification relative to the expected period of the structural features, and, the SEM was adjusted to get a very high number of pixels in the images. These SEM images were treated by software to calculate autocorrelation, FFT, and IFFT. We present how we adjusted SEM acquisition parameters for best results. We first applied our procedure on an SEM image on which the structure was obvious. Then, we applied the same procedure on a sample that must contain a periodic structure because it diffracts visible light, but on which no structure was visible on the SEM image. In both cases, we obtained clearly periodic patterns that allowed measurements of structural parameters. We also investigated how the irregularly broken surface interfered with the periodic structure to produce additional periodicity. We tested the limits of our methodology with the help of simulated images. SCANNING 36:487–499, 2014. © 2014 Wiley Periodicals, Inc.

Contract grant sponsor: Francesco Mazzero and Thomas Cenki. Contract grant sponsor: Gemoa SARL Opal Trading Company.
Conflicts of interest: None.
Address for reprints: N. Stephant, Institut des Matériaux Jean Rouxel, University of Nantes, UMR-CNRS 6502, 2 rue de la Houssiniere BP 32229, F-44322 Nantes Cedex 3, France
E-mail: nicolas.stephant@univ-nantes.fr

Received 10 January 2014; Accepted with revision 23 March 2014

DOI: 10.1002/sca.21144
Published online 17 April 2014 in Wiley Online Library (wileyonlinelibrary.com).

Key words: SEM, scanning microscope, FFT, IFFT, autocorrelation, opal, photonic crystal, silica particles, close-packed arrangements

Introduction

We present a procedure to reveal periodicity on scanning electron microscope (SEM) images where a periodic pattern is expected, but is *not* observed. To our knowledge, this has never been done on SEM images. We finalized this method to explore the structure of natural precious opals. They must have periodic structure since they diffract visible light; the patches of pure colors that move around the stone as the stone is turned are visible to the naked eye. Visible light is diffracted by opals because they are made of a regular network of silica spheres or lepispheres 150–400 nm in diameter (Sanders, '75; Gaillou *et al*., 2008). However, when observing a fresh break of a precious opal, the periodic pattern is not visible because the silica spheres are most often cemented by hydrous silica (Fritsch *et al*., 2006). Until now, for those opals, observing the periodic pattern using an SEM requires a previous chemical etching of the surface. Ideally, an hydrofluoric acid etching preferentially dissolves the cement and reveals the spheres but this operation does not always discriminate well between cement and spheres because their chemical composition is too similar (the efficiency of the method depends strongly on relative densities of the cement and spheres). That is why, even when the acid etching is correctly applied, the opals investigated here do not display periodic structure, but a more or less damaged surface. Therefore, we developed a procedure of image analysis using FFT to extract any periodic distribution of smooth discontinuities at the surface of the sample. This procedure can therefore avoid possible alteration of the true periodic pattern of the sample by the previously required acid etching treatment.

First, we improved empirically the quality of the FFT obtained from an SEM image by optimizing the parameters of image acquisition. This resulted in FFT resolution sufficient for IFFT calculation that resulted in visualization of the regular stacking of silica spheres. Finally, FFT and IFFT images allowed us to measure average size of the spheres and to visualize both the surface steps due to surface breakage and the alternation of successive, different layers making up the samples.

Fourier transformation was applied few times to SEM images for observation of photonics crystals (Shklover *et al*., 2006; Chiappini *et al*., 2009; Rusen *et al*., 2011) or opals (Viti and Gemmi, 2009) but only to confirm periodicity of a structure already observed on an image and with rather poor resolution. We attempted to find optimum conditions of SEM image acquisition to get fine resolution of an FFT image. This quality is essential to calculate a usable IFFT image. This criterion was probably never reached before this work and can explain why IFFT is never used with SEM images.

State of the Art

FFT

Many scientific publications use the mathematical function known as Fourier transformation.

Fourier transform allows conversion of SEM images into phase space. The signal is split onto elementary sinusoidal signals and shown as a new type of image where the center is the place of low frequencies and borders are places of high frequencies of the signal. This new image reveals periodic features as bright spots on the Fourier space pattern.

With appropriate software, the observed spots that correspond to periodic elements can be selected and separated from the continuous background that comes from random events at the sample surface through the use of a masking tool. When an inverse Fourier transformation is applied through this mask, only the selected periodicities contribute to the reconstructed image. In particular, the randomly distributed features are eliminated.

When applied to discrete signal, like an SEM image, Fourier transformation is more accurately called discrete Fourier transformation (DFT). An SEM image file is an integer array of m lines and n columns. Thus, the discrete Fourier transform of the image is given by (Aubert and Lecomte, 2007):

$$F(h,k) = \sum_{n=0}^{N-1}\sum_{m=0}^{N-1} I(n,m)e^{\frac{2\pi i(h\cdot n+k\cdot n)}{N}} \qquad (1)$$

And inverse discrete Fourier transform (IDFT) is given by:

$$I(n,m) = \frac{1}{N^2}\sum_{h=N/2}^{(N/2)-1}\sum_{k=N/2}^{(N/2)-1} F(h,k)e^{\frac{2\pi i(h\cdot n+k\cdot n)}{N}} \qquad (2)$$

IFFT images do not represent reality as original SEM images do, but are only representations of combined periodic signals.

The size of one pixel is the shortest measurable distance in such digital SEM images and the maximum measurable distance is the image size itself. This range of distances becomes a range of periodicities in phase space where the highest detectable frequency will be imposed by the size of the pixel of the SEM image. In other words:

$$\mathrm{FFTHFL} = \frac{1}{\mathrm{PS}} \qquad (3)$$

where FFTHFL is the FFT highest frequency limit and PS is the SEM image pixel size.

On the other hand, the lowest detectable frequency will be imposed by the size of the SEM image as this gives the longest measurable distance on the image.

In practice, an algorithm, called fast Fourier transform (FFT) is used to calculate DFT. It was proposed by Cooley and Tukey ('65) to decrease computing time by reducing the number of multiplications during calculation (Duhamel and Vetterli, '90).

Autocorrelation

Autocorrelation function compares a signal with itself after a time delay (τ):

$$R(\tau) = \int_{-\infty}^{+\infty} f(t)f(t+\tau)dt \qquad (4)$$

The result is a new image where periodic components are reinforced and noise is reduced. *Digital Micrograph* software calculates this function in this way: first, the FFT of an SEM image is calculated then multiplied by its complex conjugate. Finally, IFFT is calculated from this result and normalized to 1 (Wanner *et al*., 2008).

Close Packing in the Opal Structure

The opal structure is based on the close-packing of spheres model that was the subject of the Kepler conjecture (Hales, 2005). According to this model, congruent spheres are distributed on successive layers with a regular hexagonal arrangement within each layer. Depending on the stacking of successive layers, two possible structures are observed: the ABAB stack results in hexagonal close-packing (hcp) whereas ABCABC

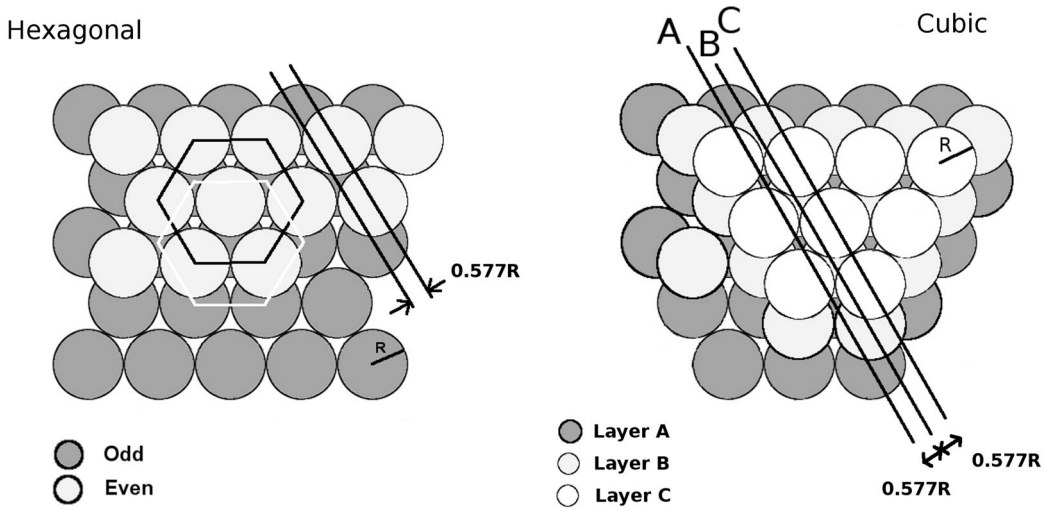

Fig 1. Visualization of two characteristic properties of close-packed structures: 1: There is a shift between two consecutive layers as highlighted by the two hexagons on the left. 2: Along each of the three directions of the hexagon, the misalignment value between two superimposed rows of spheres is 0.577 of a sphere radius.

stacking is cubic close-packing (ccp). The hexagonal close-packing model contains two families of layers shifted relative to one another. We shall call them odd and even families as they lie alternatively on the material (Fig. 1). Cubic close-packing model contains three families of layers. For both models all layers of a same family are aligned together. The magnitude of shift between layers of two consecutive families is 0.577 of a sphere radius (Fig. 1). SEM images of materials with either structure should reveal hexagonal symmetry when FFT is applied.

Materials and Methods

Materials

Sample A is a natural play-of-color opal from Australia. Secondary electron SEM images on a fresh break reveal a very clear network of silica spheres. It serves as a reference sample to test our method and its results (Fig. 2(A)).

Sample B is a play-of-color opal from Wollo, Ethiopia. The presence of play-of-color in the whole

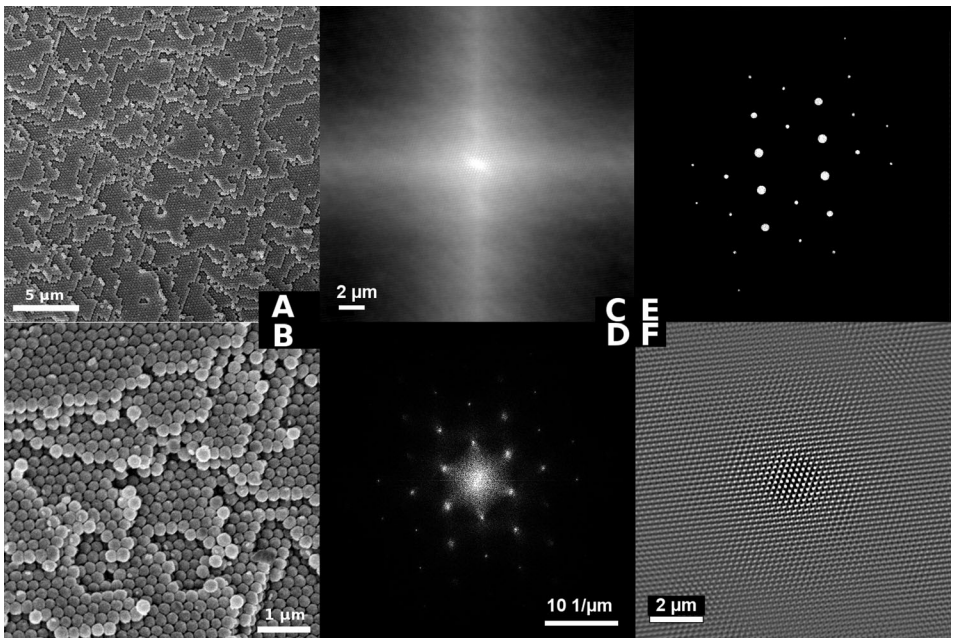

Fig 2. Our image treatment method applied to sample A. (A) Original SEM image that clearly displays a very regular network of silica spheres about 200 nm in diameter; (B) enlarged view; (C) autocorrelation of the SEM image; (D) FFT of the autocorrelation; (E) mask from the FFT; (F) IFFT from the mask.

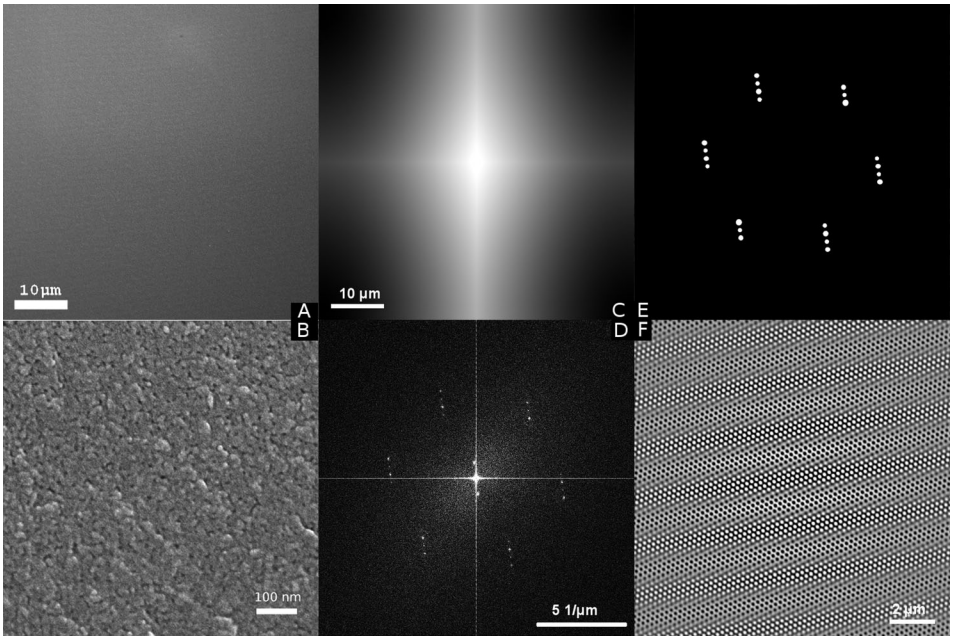

Fig 3. Our image treatment method applied to sample B. (A) Original SEM image; (B) enlarged view; (C) autocorrelation of the SEM image; (D) FFT of the autocorrelation; (E) mask from the FFT; (F) IFFT from the mask.

sample indicates that it is made of a regular packing of silica spheres in the range 150–300 nm (Sanders, '75) extending over the entire sample. SEM images show an apparently flat surface with no visible regular network (Fig. 3(A)). However the consistent play-of-color let us consider that the structure we examine by SEM is regular over the whole image.

Adjustment of SEM Parameters

Before image acquisition, several parameters must be adjusted to optimize the detection of regular patterns by the FFT. The FFT highest frequency limit should be in the right range otherwise the spot corresponding to the expected pattern will not be highlighted on the FFT. Hence, one must define a range of expected pattern dimensions before acquiring the image. Therefore, all parameters affecting the image's pixel size (PS) have to be chosen carefully. These include the magnification (M), the number of pixels (NP) in the width of the image, the real distance along image width (image size, IS), and the physical width of the picture on the screen (screen size, SS). The relationship between these parameters is the following:

$$\mathrm{PS} = \frac{\mathrm{IS}}{\mathrm{NP}} \tag{5}$$

$$\mathrm{IS} = \frac{\mathrm{SS}}{\mathrm{M}} \tag{6}$$

From (5) and (6), it results that

$$\mathrm{PS} = \frac{\mathrm{SS}}{\mathrm{M} \times \mathrm{NP}} \tag{7}$$

From (7) and (3), comes

$$\mathrm{FFTHFL} = \frac{\mathrm{M} \times \mathrm{NP}}{\mathrm{SS}} \tag{8}$$

The screen width (SS) is a constant belonging to the microscope. The magnification (M) and the image resolution (NP) are both adjustable by the operator. Their ratio should be carefully chosen before image acquisition according to the pattern periodicity expected in the sample. Insufficiently optimized parameters may lead to a black FFT were no spots can be seen except a central spot. This means also that only a small window on the magnification scale is valid for the approach to work.

To prevent this problem we established several curves (Fig. 4) indicating the optimum magnification (M) and number of pixels (NP) in the image width according to a size of pattern in the sample. A higher NP value gives better results. These curves are valid for our JEOL7600F SEM and can be calculated for any other microscope by entering the correct screen size (SS) in Equation (8).

Experimental Procedure

Opal samples were imaged using an SEM JEOL JSM 7600F equipped with a thermal field emission gun. Samples were freshly broken fragments coated with

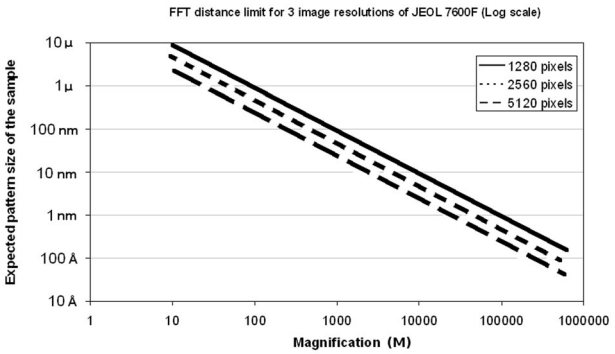

Fig 4. Curves for optimized adjustment of magnification and the number of pixels (NP) in the image width, according to Equation (8), for a range of pattern sizes. These curves allow a rapid choice of SEM image acquisition parameters if the size range of the pattern is known. These curves are established for a JEOL 7600F SEM.

15 Å of platinum to ensure electrical conductivity at the sample surface. They were placed on the SEM stage as horizontally as possible. According to the considerations given above and to get acceptable resolution of FFT and IFFT pictures, we selected the highest image resolution of our SEM (5,120 pixels) and slowest scan speed in photo mode when possible. The magnification was determined using Figure 4. All images were taken using the secondary electron detector.

Each image was treated using *Digital Micrograph* (Gatan, Inc., Pleasanton, CA). After distance calibration, we first calculated an autocorrelation image of the SEM image to strengthen information about periodicity in the SEM image. The FFT was then calculated from the autocorrelation image. This result is also called PSD for Power Spectral Density (Prandoni and Vetterli, 2008). When we observed bright spots on the FFT (that represent periodicities), we selected them using a mask and then launched the IFFT based on these spots only. We obtained a filtered image highlighting the periodic information only. This final image must be understood as a graphic representation of all periodic matters inside the initial SEM image, but not as an SEM image where only the non-periodic features were removed. We also created masks selecting only targeted spots on the FFT to determine which components of the whole sample pattern gave rise to the final IFFT image.

In the resulting IFFT images, all periodic patterns extend over the whole surface of the image although they can originate from different regions in the original SEM image. In order to highlight this phenomenon, we constructed an artificial image with a clearly periodic structure on which we added a heterogeneity in the middle—we chose a mushroom (Fig. 5). Then, we launched our procedure (bottom row of images) and the same procedure but without the auto-correlation step (top row). In both final IFFT images, a pattern is present

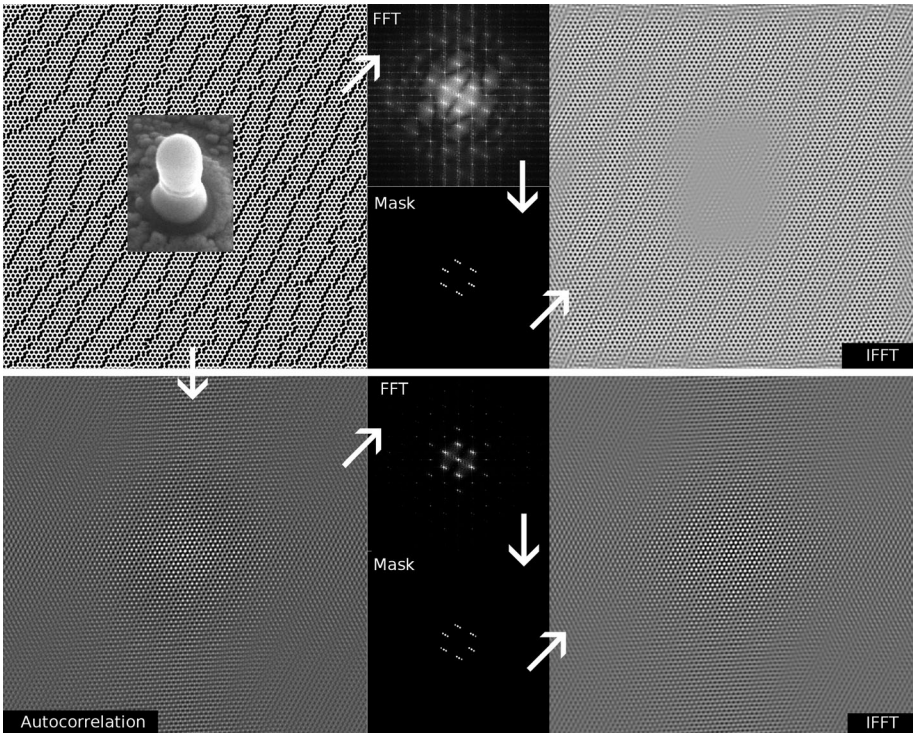

Fig 5. An artificial image (top left) treated with our method (bottom row: autocorrelation, FFT, mask, IFFT) and without the autocorrelation step (top row). In both resulting IFFT images, a periodic pattern is observed in the middle of the image when there was not one in the original image. Our method reveals periodic patterns, but not heterogeneities or singularities. The periodicity is perfectly clear only when autocorrelation is included.

in the center of the IFFT image, although this does not correspond to reality. This shows that the method we developed reveals periodic patterns, but not inhomogeneities or singularities.

We measured distances on the FFT images using the profile tool of *Digital Micrograph* (Gatan, Inc.).

Results

Tests on a Previously Known Periodic Structure (Sample A) and a Glass Shard

Regular close-packed layers in sample A are already clearly visible on the SEM image even at low magnification (Fig. 2(A) and (B)). The FFT of the autocorrelated image (Fig. 2(C) and (D)) shows spots due to this periodic pattern. By selection of those spots with the masking tool of *Digital Micrograph* we obtained a filtered FFT pattern from which we calculated the IFFT (Fig. 2(E) and (F)). Despite a slight distortion due to the sample tilt at the time of acquisition, the FFT also shows a hexagonal symmetry (Fig. 2(D)).

The average sphere diameter can be deduced from the distances between adjacent rows, evaluated from the spot positions on the FFT. Three values were collected along the three directions, and then averaged (Fig. 6). Then we divided this result by $\sqrt{3}/2$ to get the diameter of the spheres. This calculated mean value is consistent with the mean value obtained from the measurement of a row of ten spheres directly on the SEM image (Table I).

The directions and sizes of the patterns are perfectly consistent between the SEM image and the IFFT (Fig. 7). This demonstrates that our calculation method does correctly represent reality, does not add periodic patterns artificially, nor does it loose information.

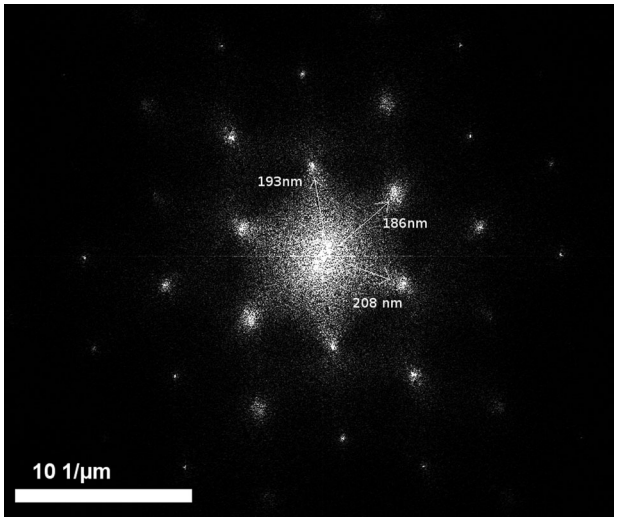

Fig 6. Distance measurement of the periodic pattern. Three values, one from each direction of symmetry, allow the calculation of the average size of the spheres.

We also acquired, under the same conditions, an SEM picture of a glass shard that has no periodic structure. Then we launched the image treatment procedure. The FFT image did not reveal any periodic structure in the glass (Fig. 7(B)). This again demonstrates that our procedure does not reveal a periodic structure where there is none in reality.

Observation of Materials With Hidden Periodic Structure (Sample B)

When sample B was fractured, the shock wave produced successive stairs revealing many layers across the SEM image; this phenomenon is perceptible on the enlarged view of the SEM image (Fig. 8, left inset) and highlighted (Fig. 8, right inset) by the measure obtained with the profile tool of *Digital Micrograph*. This measure was made with the image used to calculate the FFT and the IFFT. Otherwise, the surface appears nearly flat. Nevertheless the FFT of the autocorrelated image clearly reveals a hexagonal pattern (Fig. 3(D)).

This global pattern is obviously due to the tridimensional arrangement of silica spheres. However, unlike the previous sample, additional spots are observed. The fracture, realized randomly through the opal rough, appears to develop along a vicinal plane, near a dense basal plane. This section crosses the stack of layers, giving rise to successive and almost periodic bands or steps, like stairs. The two additional spots near the center of the FFT give the average distance between these stairs (1.14 µm; Fig. 9). This value is consistent with the steps observed on the initial SEM image (Fig. 8).

The period due to the stairs also combines with the sixfold pattern, as shown in Figure 9(E). Among the six groups of spots, two show three spots aligned along the stair direction, and the four others show four spots in the stair direction. Hence, among each group, some spots arise from the network of silica spheres, and others arise from the stairs. However it is quite difficult to discriminate between these origins.

We first considered that the most regular hexagonal pattern was due to the silica sphere network (Fig. 10). We used these three pairs of spots to calculate the diameter of the spheres by measuring the distance between spots and the center along the three resulting directions on the FFT (Fig. 10). As before, we divided this result by $\sqrt{3}/2$ to get the sphere diameter (Table II).

Despite the presence of siliceous cement, the IFFT (Fig. 3(F)) reveals a very regular sixfold symmetry analogous to that of sample A. However, the nearly horizontal bands about 1 µm in size are clear effects of the stairs. Subsequently, we will refer to this IFFT as "global IFFT." In order to avoid this effect, we decided to calculate a new IFFT based on six spots only, one per group, using a new mask. This last image may be

TABLE I Calculation of sphere diameter from the FFT periodic pattern compared to direct measurement of a row of ten spheres on the SEM image

First direction	Second direction	Third direction	FFT (average)	SEM image (average of 10 measurements)
223 nm	215 nm	240 nm	226 nm	225 nm

understood as the result of a filter that selects only the periodic pattern due to the arrangement of the spheres in any single close-packed layer family A, B, or C. We chose the spots that gave the most regular hexagonal pattern on the FFT. Empirically working on FFT with *Digital Micrograph* we found that only four combinations of spots are valid patterns. The aspect of each IFFT result and symmetry of hexagonal pattern on FFT lead us to select only one combination (Fig. 11). This was the only image where no effect of the stair arrangement can be seen on IFFT. We call further this IFTT "spheres IFFT."

To determine where exactly the borders of the stairs on the global IFFT are, we drew an image that is a

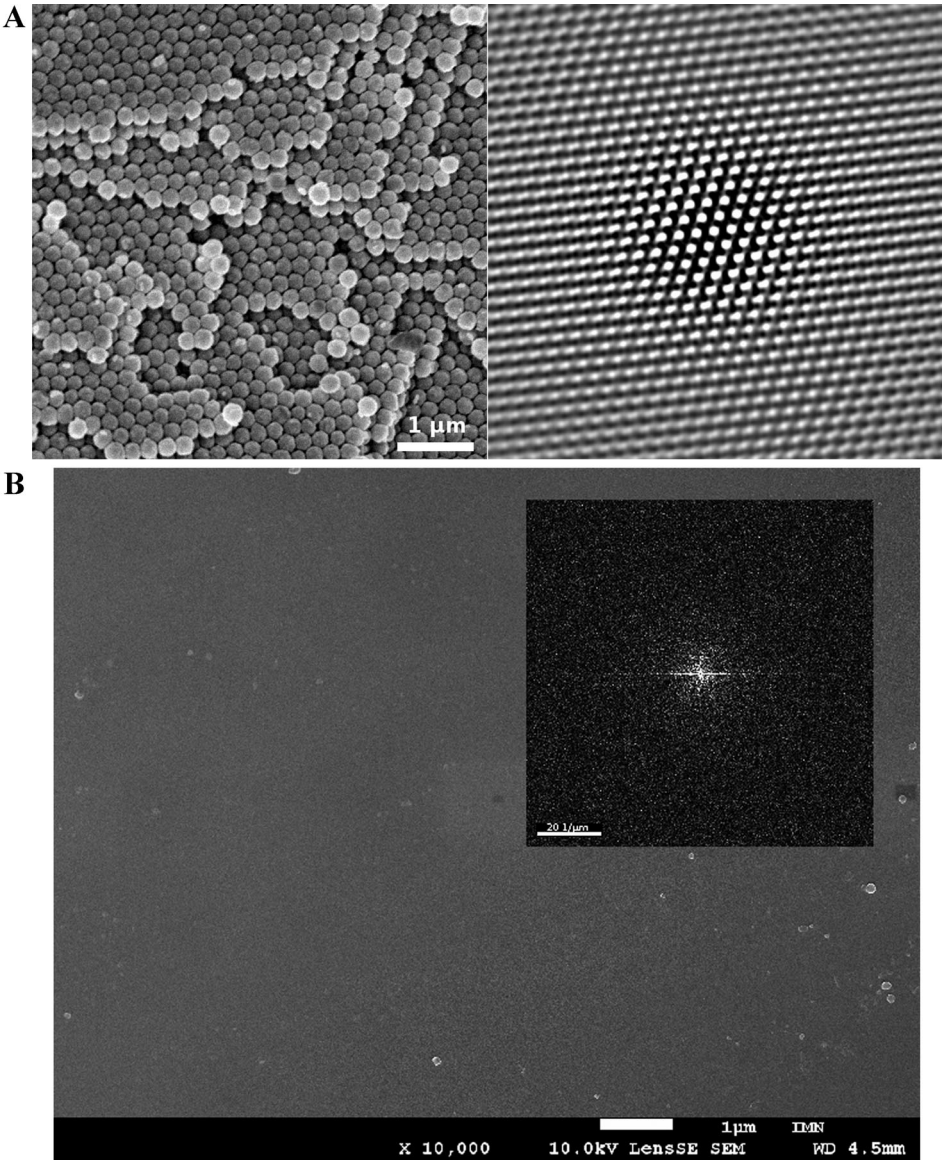

Fig 7. (A) Detail of the IFFT is superimposed onto the corresponding area of the SEM image for comparison. The position of the spheres and the orientation of the pattern are the same. (B) SEM image of a glass shard and resulting FFT by our method. No evidence of periodicity can be seen in this amorphous material.

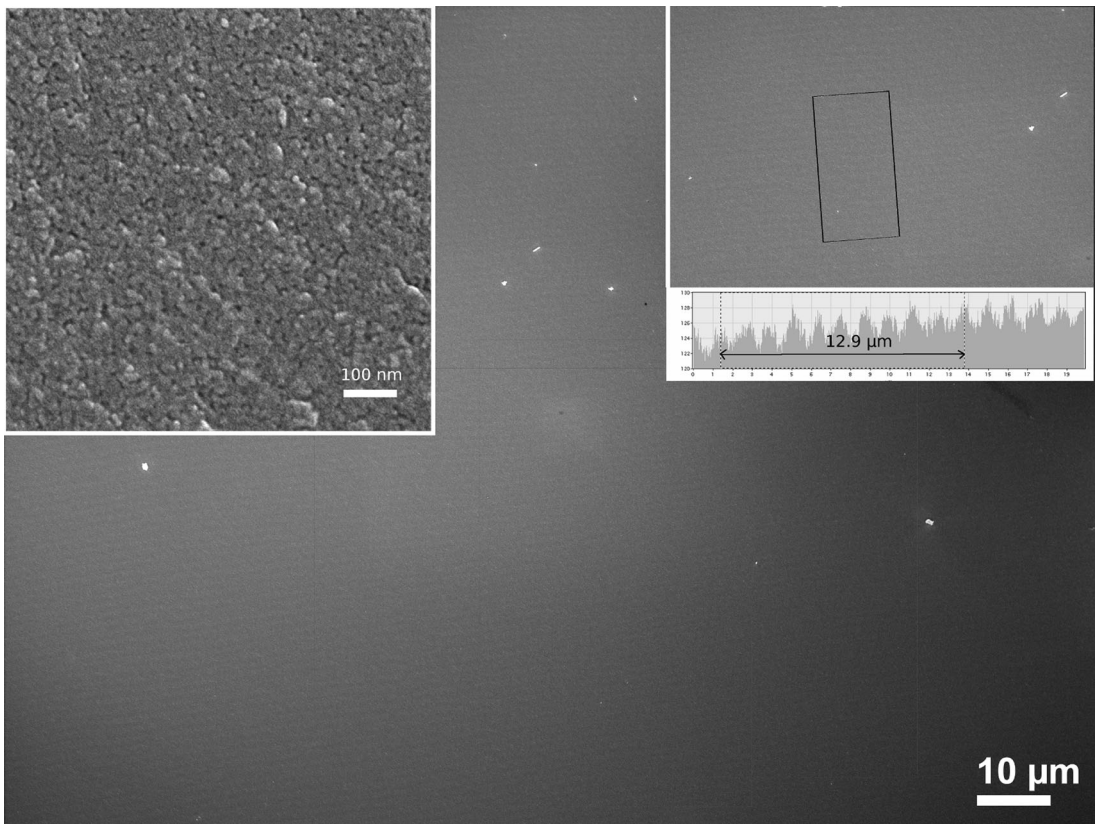

Fig 8. The SEM image of sample B used for FFT calculation. Left inset is high magnification image of the surface. The profile on the right inset highlights existence of stairs. An average size was calculated for 10 steps.

simulation of hexagonal close-packed sample crossed by vertical stairs and we treated it by our method (Fig. 12). This shows that each band, either dark or bright, is representative of one stair.

To simulate the duplication of a given periodic pattern by stairs, we built two artificial images that could resemble the case of sample B: the first shows a hexagonal close-packed pattern and the second is a

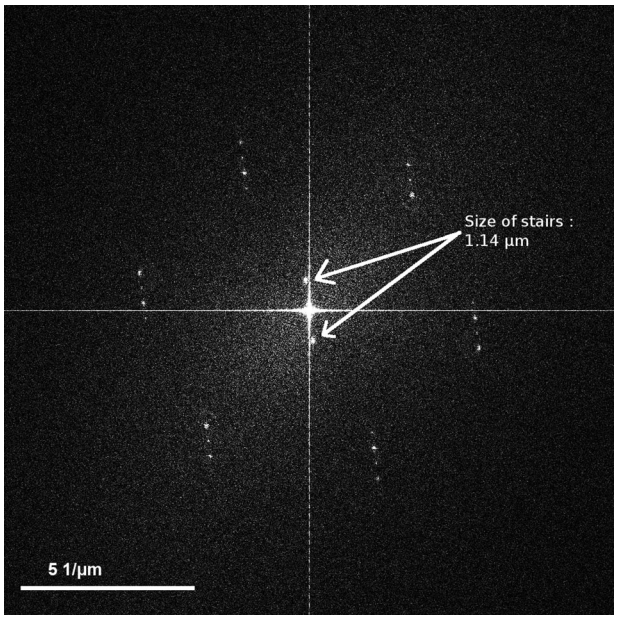

Fig 9. On sample B, the stair distribution is regular enough to induce two spots near the center of the FFT. We calculated an average size of the stairs of 1.14 µm.

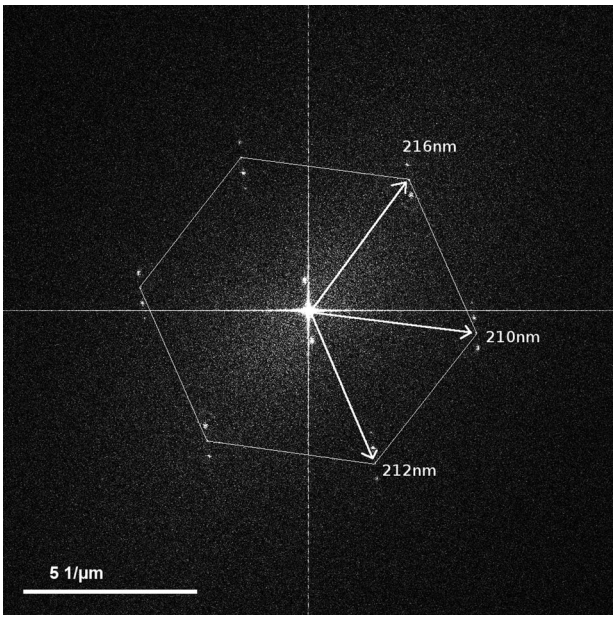

Fig 10. The distance between the spots and the center indicate the width of the rows of spheres. The structure clearly has hexagonal symmetry.

TABLE II Calculation of the average sphere diameter in sample B from the most regular hexagonal pattern of the FFT

First direction	Second direction	Third direction	Average
249.4 nm	242.5 nm	244.8 nm	245.6 nm

cubic close-packed pattern; both contain stairs (Fig. 13, left column). Then we applied our procedure (autocorrelation, FFT, mask, IFFT). The FFT (middle column) clearly shows the sixfold symmetry of the hexagonal pattern, and shows that both periods (stairs and spheres) combine and give rise to additional spots. The two IFFT images (right column) are very similar. Hence discrimination between the two structures is not obvious nor is determination of the structure of Sample B (compare with Fig. 3(F)).

To check the validity of the information visible on the IFFT image we used our simulations to compare autocorrelation images with IFFT images (Fig. 14). Even for our artificial images which are nevertheless simple cases (compared with the real samples) there is a loss of information about layer families as the procedure progresses from the autocorrelation to the IFFT.

Discussion

Play-of-Color Opal Without Siliceous Cement (Hexagonal Close-Packed Sample A)

Our sample was broken oblique to the packing direction providing a terraced configuration that shows several layers of alternating even and odd families of spheres. The shift between them can be observed on the SEM image (Fig. 15); a line drawn across several layers through the middle of spheres of one kind of layer family (odd or even) passes nearly between two lines of spheres

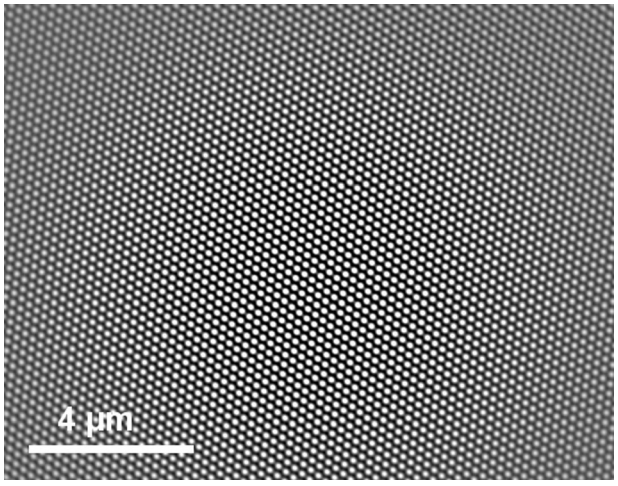

Fig 11. Structure of one layer of spheres (spheres IFFT, see text) without the stairs effect due to breaking.

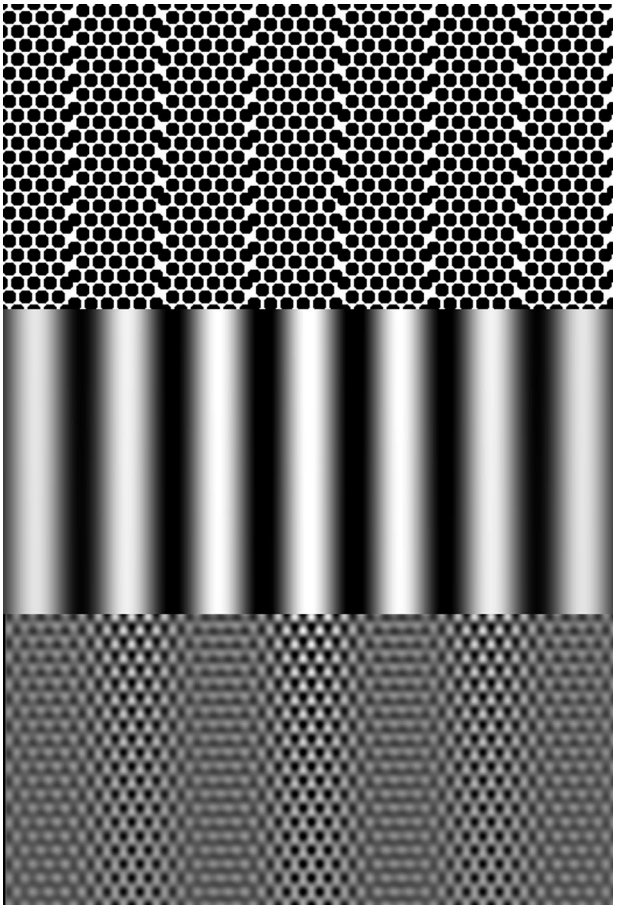

Fig 12. Top: Detail of our simulation highlighting regular vertical. Center: IFFT image calculated for an adjacent ROI (region of interest) and for the nearest spots from FFT center that arise from the stairs. Bottom: IFFT image calculated for the next adjacent ROI when all FFT spots are selected except both spots near the center. One stair of the top image is consistent with the assembly of one bright line and one dark line of center image. Each line of the bottom image, dark or bright, is also representative of a stair.

of the next layer (Fig. 15). Theoretically this shift is 0.577 of a sphere radius but very precise measurement cannot be done here because of the sample tilt conditions and relative packing orientation: the calculation is perturbed by the perspective effect.

The FFT shows hexagonal symmetry, as expected (Fig. 2(D)) but, because the two patterns are equal in direction and parameters, the image cannot discriminate between odd and even layers.

On the other hand, IFFT clearly reveals both families, odd and even (Fig. 16). They are distinguished by the two interlaced hexagonal patterns. As previously stated, the IFFT repeats over the whole image all periodic patterns although they are spatially separated on the initial SEM image.

Applied to more complex structures, interpretation of IFFT will be more difficult if respective layer positions are too close together and/or the sample structure contains more layers.

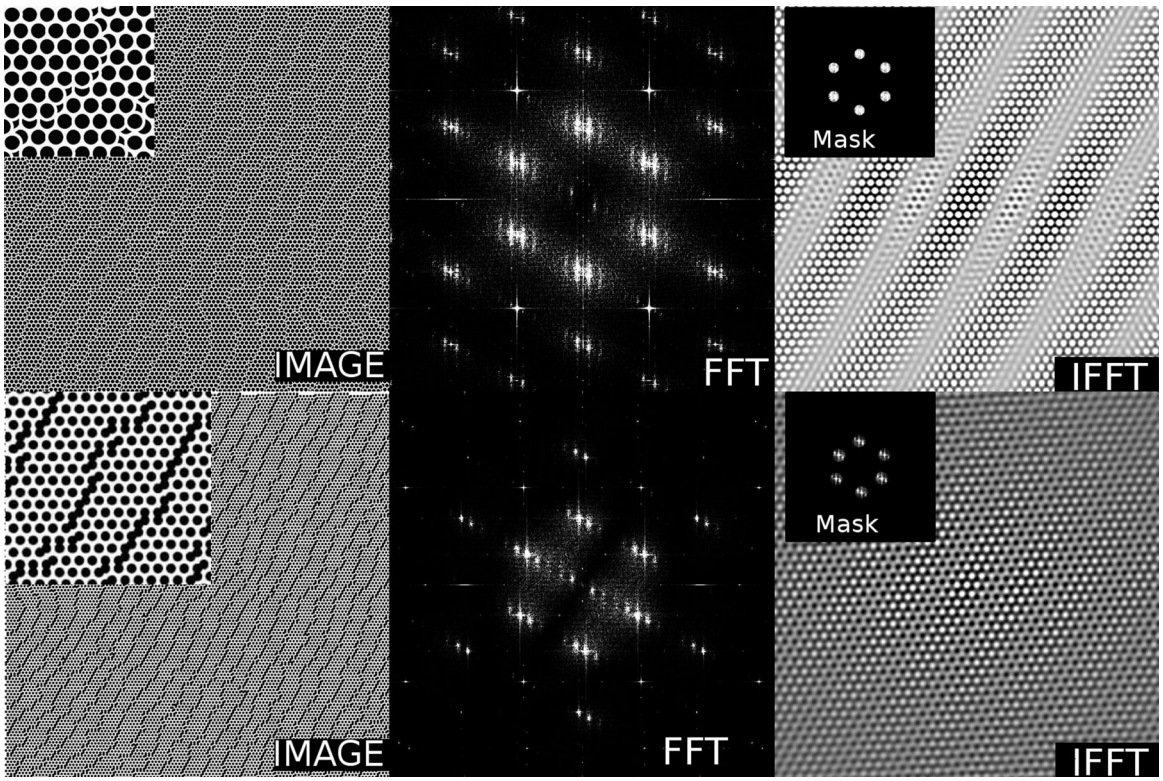

Fig 13. First column: Simulations of stairs superimposed onto a regular close-packed network and resulting FFT (second column), mask and IFFT (third column). The first row is a hexagonal close-packed arrangement and the second row is a cubic close-packed arrangement.

FFT is useful to provide a distance measurement of thousands of spheres contained on the low magnification image, and hence an average size. This value cannot be calculated as easily over a so large number of spheres on the SEM image because a higher magnification is required. In spite of imperfections on the surface of our sample, we calculated a value consistent with that measured on the initial image.

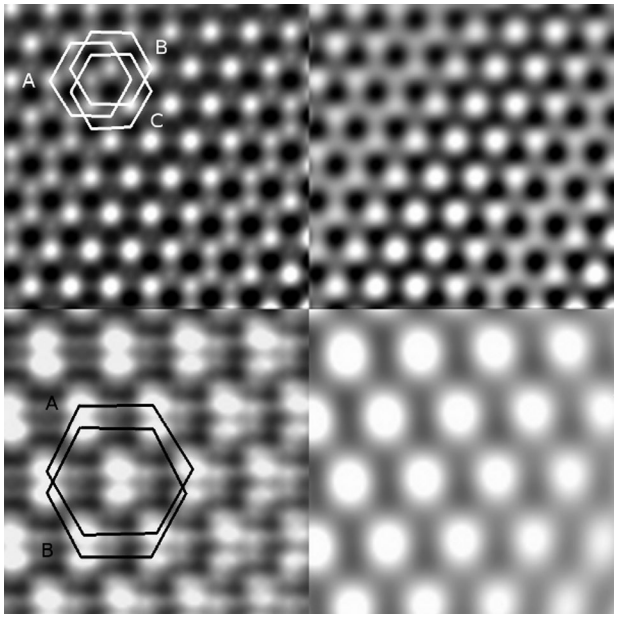

Fig 14. Autocorrelation (first column) and IFFT (second column) from simulated images in the case of cubic close packing (top row) and hexagonal close packing (bottom row). Information showing the existence of layer families is visible on the autocorrelation images but not on the IFFT images.

Play-of-Color Opal With Siliceous Cement (Sample B)

This sample has a similar layer structure to sample A but the spheres are encapsulated in siliceous cement. As

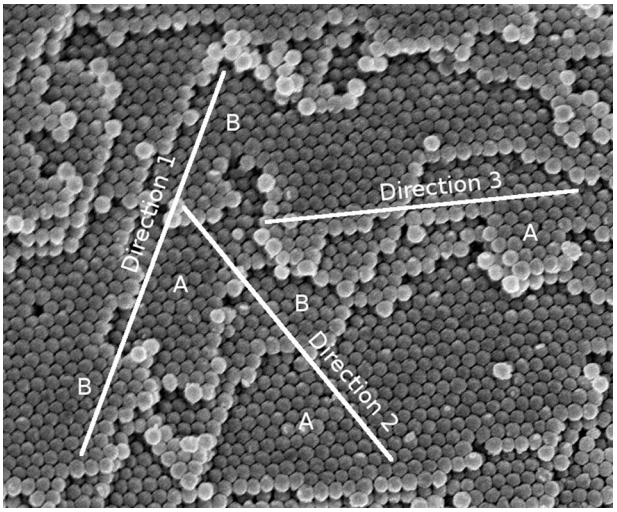

Fig 15. Detail of the SEM image of play-of-color opal sample A. For the three directions, all rows in A-type layers are aligned together and shifted from those in B-type layers.

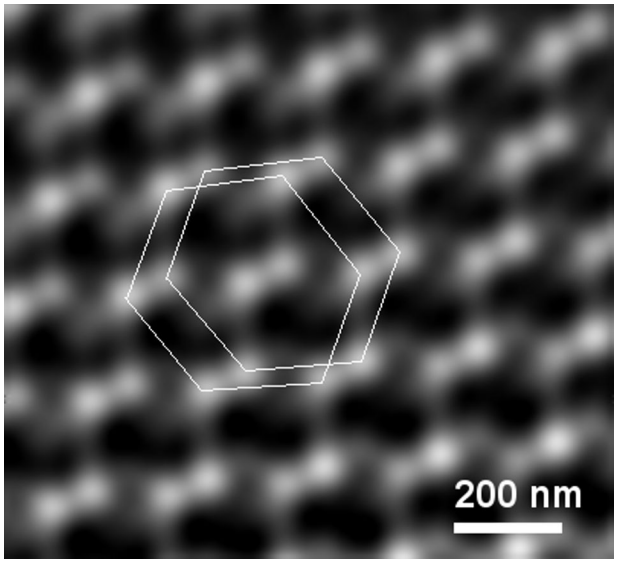

Fig 16. Interlaced odd and even pattern on the IFFT of sample A.

a result, no evidence of a regular structure can be seen on the SEM image. An image made at higher magnification (Fig. 3(B)) reveals details on whole surface but does not allow characterization of the structure because of the state of the surface (mainly because of the featureless silica cement).

Nevertheless, the FFT of B (Fig. 3(D)) revealed a hexagonal symmetry proving that our initial SEM image contains hidden information about the sample structure.

This means that Fourier transformation is able to detect periodicity within the pixels of the SEM image. This is possible mainly for two reasons: At first the excellent resolution of the pixel size of the image that was fixed by the acquisition parameters and also because cement and spheres in the material are slightly different in terms of density that causes contrast detectable by the FFT calculation.

The siliceous cement and the stair structure render this surface less regular than the one of the previous sample. This interrupts the lattice-of-spheres arrangement and explains the absence of higher-order spots.

Two main patterns are superimposed on the global IFFT, the first from the sphere arrangement and the second from breaking conditions that resulted in stairs on the sample surface. This may cause confusion for interpretation of the IFFT because the sphere pattern contrast is strongly modulated by the contrast of the stair pattern signal.

IFFT cannot show a real view of the stair habit and distribution in the studied area. A high-magnification view of the surface (Fig. 8, left inset) shows stairs irregular in direction and size, but our measurement is made on a much larger surface and it highlights a large-scale, average regularity. On the same image as that was used for our calculations, a profile using *Digital Micrograph* highlights a periodic change of contrast on the surface. The measure over ten steps gives 12.9 μm, hence 1.29 μm per step, that is fairly consistent with the one calculated by our method (1.14 μm). The difference may be explained by some irregularity of the steps over the whole image. In this case, FFT and IFFT together give quantitative information that cannot be obtained with only the SEM image.

The spheres IFFT (Fig. 11) clearly reveals the sphere arrangement within one layer. This result is quite surprising considering uniformity and lack of obvious information on the original SEM image. However, interpretation of what is seen on global IFFT and spheres IFFT is not straightforward because preliminary knowledge of the structure is missing and the uniformity of the surface complicates interpretation of the results. We cannot determine the sequence of the stacking in terms of A, B, and C layers because discrimination between layer families is not evident as it was in sample A. We decided to build simulated images (Fig. 13) to better understand what is really shown on the IFFT image. On the FFT images of our simulations, we observe both spots due to the stairs and superstructure spots so the simulations mimic our observations. Simulated images confirm the difficulty when an additional strong periodic signal is present as the stairs. Neither the IFFT of a simulated image for cubic close-packed nor for hexagonal close-packed (Fig. 13) can distinguish between A, B, or C families as it did for sample A (Fig. 16). All the resulting spots of those families are superimposed on the FFT and their intensities can be strongly modified by an additive signal from alternating bands (like the stairs) that can obscure the fine information contained inside.

We wanted also to check if our procedure induces artifacts on the final IFFT, including possible loss of information on periods as a result of the multi-step procedure. For that, the autocorrelation image calculated from a real SEM image where no evidence of structure can be seen is not usable, but one calculated from our simulated images is (Fig. 14). Autocorrelation is a particular case of IFFT so we can compare directly an IFFT obtained at the end of our method and the corresponding autocorrelated image. This comparison (Fig. 14) clearly demonstrates that information is lost during the multi-step process. In the case of hexagonal close-packed simulated image, coexistence of A and B families is clearly visible on the autocorrelation image where two patterns are nearly superimposed. Each spot of one family is very close to a spot of the other family. This proximity causes misinterpretation when autocorrelation is submitted to FFT then IFFT. Nearby spots on the autocorrelation are merged together on the IFFT to create a new bigger spot. The same problem is also seen in case of cubic close-packed simulated image. Six spots

arranged as a hexagon highlight the existence of A, B, and C families on the autocorrelation image but only one family is visible on the IFFT. This phenomenon is caused by insufficient pixel resolution on the original SEM image that is propagated and amplified through the subsequent steps of the treatment. This is also a limitation to our method that can be reduced by choosing the best pixel resolution of the SEM whenever possible. Modern SEMs have a range of pixel resolutions, and, unfortunately, some are too low for this procedure. The pixel resolution will probably increase in the future thus increasing the applicability of this method.

Accordingly, to improve the resulting images, not only the size of the spheres has to be considered but also the relative position between spheres from different families of layers.

Despite siliceous cement which hides the sphere pattern of sample B and the limitations described above, we confirmed the existence of a regular structure as was expected because of the play of colors, we observed its symmetry, and we measured the average size of the silica spheres.

Further work on this procedure could include the creation of software tools to construct simulated SEM images for comparison with real SEM images or the creation of a library of IFFTs from different types of structures as references.

Conclusion, Perspectives

In an unusual way, scanning electron microscopy was successfully used to investigate the periodic structure of play-of-color opals. We developed a methodology to calculate image acquisition parameters to get appropriate image resolution. The resulting SEM images were treated with dedicated software to get FFT images and IFFT images.

This technique was first tested on a reference opal sample that clearly shows a periodic structure on the SEM image to demonstrate that the procedure gives results consistent with the direct observation. Then the procedure was applied to another opal sample from which no periodic structure can be seen on an SEM image. The IFFT image clearly revealed a periodic structure in this second sample.

Results on both samples are consistent. Hidden or not, the structure of opal is revealed even when surface conditions prohibit collection of structure parameters directly.

In addition, information about breaking habits were revealed, such as parallel stairs that arise from the combination of the oblique breaking plane with the periodic structure of the opal. By the method presented herein, we obtained more information about the surfaces of our broken samples than observing traditional SEM images alone. Also, FFT allows precise measurement of an average silica sphere diameter from a very large sampling of many spheres.

The limitations of the methodology arise from the initial resolution of the SEM image because the pixel resolution of the SEM has to be as high as possible to clearly visualize smallest parameters of the sample pattern. It is these fine details that can be lost during successive calculations.

This methodology allowed us to simplify opal sample preparation and to observe a surface without preliminary etching with hydrofluoric acid, a traditional method for investigating the periodic structure in opals. Here, we avoid the sphere damage that can be caused by the chemical etch.

Our method reveals periodic patterns in apparently homogeneous images, and allows measurement of periodicity parameters (distance between patterns). However, we encountered difficulties in determining the exact 3D structure of our samples. This shows that further development in structure analysis is necessary, through simulation or analysis of well-known structures, to improve structure determination.

We believe that our method is applicable for observation of natural or synthetic materials presenting such periodic structures as, for example, photonic crystals. In addition, it may be used to investigate the propagation of shock waves in periodically structured materials.

Acknowledgments

We thank Nicolas Gautier, Institut des Matériaux Jean Rouxel, Nantes, France, for the help in preliminary sample preparation tests. This work was supported by Francesco Mazzero and Thomas Cenki, Gemoa SARL Opal Trading Company, who provided the play-of-color samples.

References

Aubert E, Lecomte C. 2007. Illustrated Fourier transforms for crystallography. J Appl Cryst 40:1153–1165.

Chiappini A, Armellini C, Chiasera A, *et al*. 2009. An alternative method to obtain direct opal photonic crystal structures. J Non-Cryst Solids 355:1167–1170.

Cooley JW, Tukey JW. 1965. An algorithm for the machine calculation of complex Fourier series. Math Comput 19(90):297–301.

Duhamel P, Vetterli M. 1990. Fast Fourier transforms: A tutorial review and a state of the art. Signal Process 19: 259–299.

Fritsch E, Gaillou E, Rondeau B, *et al*. 2006. The nanostructure of fire opal. J Non-Cryst Solids 352:3957–3960.

Gaillou E, Fritsch E, Aguilar-Reyes B, *et al*. 2008. Common gem opal: An investigation of micro- to nano-structure. Am Mineral 93:1865–1873.

Hales TC. 2005. A proof of the Kepler conjecture. Ann Math Second Series 162(3):1065–1185.

Prandoni P, Vetterli M. 2008. Signal processing for communications. Lausanne, Switzerland: EPFL Press. p 224–227.

Rusen E, Mocanu A, Marculescu B, *et al*. 2011. Obtaining complex structures starting from monodisperse poly(styrene-co-2-hydroxyethylmethacrylate) spheres. Colloid Surf A 375:35–41.

Sanders JV. 1975. Microstructure and crystallinity of gem opals. Am Mineral 60(9–10):749–757.

Shklover V, Braginsky L, Hofmann H. 2006. Domain structure and optical properties of colloidal photonic crystal. Mater Sci Eng C26:142–148.

Viti C, Gemmi M. 2009. Nanostructures and microinfrared behavior of black opal from Gracias, Honduras. Neues Jb Miner Abh 186:11–20.

Wanner G, Vogl K, Overmann J. 2008. Ultrastructural characterization of the prokaryotic symbiosis in "*Chlorochromatium aggregatum*." J Bacteriol 190:3721–3730.